Applied Catalysis B: Environmental 127 (2012) 137–147

Contents lists available at SciVerse ScienceDirect

Applied Catalysis B: Environmental

journal homepage: www.elsevier.com/locate/apcatb

The influence of silicon on the catalytic properties of Cu/SAPO-34 for NO_x reduction by ammonia-SCR

Jun Wang[a], Tie Yu[a], Xinquan Wang[a], Gongshin Qi[c], Junjie Xue[a], Meiqing Shen[a,b,*], Wei Li[c,**]

[a] Key Laboratory for Green Chemical Technology of State Education Ministry, School of Chemical Engineering & Technology, Tianjin University, Tianjin 300072, PR China
[b] State Key Laboratory of Engines, Tianjin University, Tianjin 300072, PR China
[c] General Motors Global Research and Development, Chemical Sciences and Materials Systems Lab, 30500 Mound Road, Warren, MI 48090, USA

ARTICLE INFO

Article history:
Received 1 March 2012
Received in revised form 13 August 2012
Accepted 17 August 2012
Available online 25 August 2012

Keywords:
Cu/SAPO-34
Si content
NH_3-SCR
EPR
NMR

ABSTRACT

The effect of Si content in SAPO-34 on NO selective catalytic reduction over Cu/SAPO-34 catalyst was investigated. Three fresh catalysts with different Si contents, prepared by the same procedure, showed different NO conversions from 120 °C to 600 °C. These catalysts were characterized in detail by various techniques (ICP, XRD, SEM, NMR, NH_3-TPD, H_2-TPR and EPR). The NH_3-TPD results indicate that the number of acid sites in Cu/SAPO-34 catalyst increases with increasing Si contents and the SCR activities of the samples correlate well with the number of acidic sites at low temperatures (200 °C). The EPR and H_2-TPR results show that both the Si and the Al contents affect the number of isolated Cu^{2+} ions in Cu/SAPO-34 catalysts. The catalysts aged at 750 °C for 12 h showed higher SCR activities than those of the untreated samples, consistent with the higher numbers of the isolated Cu^{2+} ions.

1. Introduction

Currently, selective catalytic reduction (SCR) of the NO by NH_3 is one of the most efficient technologies for NO_x removal for diesel emissions control [1,2]. Many researchers have focused on the base metal exchanged-zeolites catalysts, such as Cu/ZSM-5 and Fe/beta. Cu/ZSM-5 has shown superior SCR activity and N_2 selectivity in the temperature range (200–400 °C) [2]. However, the application of Cu/ZSM-5 is limited due to its lower hydrothermal durability [3,4].

The C_3H_6-SCR activity of Cu/SAPO-34 catalyst was reported 10 years ago [5], but few studies on the NH_3-SCR activity over this material have been conducted. Recently, small pore sized molecular sieves or zeolites with CHA structure, such as SAPO-34 and SSZ-13, have received great attention due to their high thermal stability [4,6–9]. Kwak et al. [8] reported that Cu/SSZ-13 exhibited higher activity and higher N_2 selectivity during SCR temperature range (160–550 °C) compared to the Cu/ZSM-5. Cu/SAPO-34 would be also a promising SCR catalyst due to its excellent SCR activity and hydrothermal stability. Lobo [4] studied the activity of Cu/SAPO-34 catalyst and found that the NO conversion reached nearly 100% between 200 °C and 400 °C. After hydrothermal aging, the activity of Cu/SAPO-34 catalyst has been even improved.

It is well known that the acidity of the support plays an important role in NH_3-SCR reaction over zeolite type catalysts [1,2]; however, few studies have been reported on how the acidity of the SAPO-34 affects the SCR activity over Cu/SAPO-34 catalyst. So it is very interesting to study the effect of the Si content on the SCR performance since the Si content affects the acidity of the support (SAPO-34) and the Cu loading over zeolites. In this report, three Cu/SAPO-34 catalysts were prepared using SAPO-34 molecular sieves with different Si contents. And then the SCR activities were evaluated and the structures of Cu/SAPO-34 catalysts were characterized by X-ray diffraction (XRD), nuclear magnetic resonance (NMR), electron paramagnetic resonance spectroscopy (EPR) and temperature programmed reduction (TPR). Finally, the relationship between the Si content and the SCR activities over Cu/SAPO-34 catalysts was investigated and summarized.

2. Experimental

2.1. Catalyst preparation

The HSAPO-34 molecular sieves with different Si contents were supplied by Shanghai Novel Chemical Technology Company. Information about HSAPO-34 supports denoted as Si_xAl_y is shown in Table 1, where *x* and *y* are the mole percent of Si and Al in HSAPO-34, respectively. All the Cu/SAPO-34 catalysts were prepared by the

* Corresponding author at: School of Chemical Engineering and Technology, Tianjin University, 92 Weijin Road, Tianjin 300072, Nankai District, China. Tel.: +86 22 27892301; fax: +86 22 27892301.
** Corresponding author. Fax: +1 586 986 8697.
E-mail addresses: mqshen@tju.edu.cn (M. Shen), wei.1.li@gm.com (W. Li).

0926-3373/$ – see front matter © 2012 Elsevier B.V. All rights reserved.
http://dx.doi.org/10.1016/j.apcatb.2012.08.016

Table 1
Chemical composition of SAPO-34 and Cu/SAPO-34 catalysts.

Catalysts	Supports (molar composition)	Product composition			
		Si/(Si + P + Al)	Al/(Al + P + Si)	(Si + P)/Al	Cu loading (%)
$Cu_{0.769}/Si_{0.130}Al_{0.435}$	$Si_{0.130}P_{0.435}Al_{0.435}O_2$	0.130	0.435	1.299	0.769
$Cu_{1.264}/Si_{0.374}Al_{0.441}$	$Si_{0.374}P_{0.185}Al_{0.441}O_2$	0.374	0.441	1.268	1.264
$Cu_{1.122}/Si_{0.106}Al_{0.532}$	$Si_{0.106}P_{0.362}Al_{0.532}O_2$	0.106	0.532	0.880	1.122

ion-exchange method over HSAPO-34 supports as following. The NH_4-SAPO-34 molecular sieves were prepared by ion-exchange of HSAPO-34 in ammonium nitrate solution. After the pH of solution was adjusted to 3, the mixture was kept stirring at 80 °C for 3 h. The obtained slurry was filtered through a Bucher filter and washed using deionized water until the filtrate became neutral. And then the solid was dried at 90–100 °C for 16 h in oven. Cu/SAPO-34 catalysts were prepared by ion-exchange of NH_4-SAPO-34 in copper sulfate solution. The NH_4-SAPO-34 was mixed with 0.1 M copper sulfate solution and the mixture was stirred vigorously at 70 °C for 2 h. The slurry was filtered, washed and the solid was dried, and then the dried Cu/SAPO-34 was calcined at 550 °C for 4 h, and the calcined samples were called fresh Cu/SAPO-34. To investigate the stability of Cu/SAPO-34 catalysts, all the fresh Cu/SAPO-34 catalysts were hydrothermally treated at 750 °C for 12 h in 10% H_2O/air and the treated samples were called aged Cu/SAPO-34. The Cu/SAPO-34 catalysts are named as "Cu_z/Si_xAl_y" shown in Table 1, where z is the Cu loading by weight percent.

2.2. NH_3-SCR performance evaluation

The SCR activity was tested in a stainless steel reactor using 0.5 g catalysts mixed with 1.5 g quartz. The catalyst was sealed in the tube with quartz wool. The temperature was controlled by a type K thermocouple inserted into the center of the powder catalyst. The inlet gas composition was controlled by several mass flow controllers. FTIR (Nicolet IS10) was used to measure the concentration of NO, NO_2, N_2O and NH_3. The gas flow and the space velocity in all experiments were controlled at 1000 ml/min and 35,000 h^{-1}, respectively. Prior to the experiment, the catalysts were heated up to 500 °C and kept at 500 °C for 10 min under 5% O_2 in N_2. All experiments were performed at atmospheric pressure and nitrogen as balance. Steady-state activity tests were performed for all catalysts in the absence of water using a feed gas composition of 500 ppm NO, 500 ppm NH_3 and 5% O_2. In addition, the activity tests with 5% H_2O were performed over Cu/SAPO-34 samples. The tested temperature was from 120 °C to 600 °C, including 11 temperature points of 120 °C, 150 °C, 200 °C, 250 °C, 300 °C, 350 °C, 400 °C, 450 °C, 500 °C, 550 °C, 600 °C, respectively. At each temperature, the experiment data were recorded after NO and NH_3 concentrations were stable. The NO and NH_3 conversions were calculated by the following equations:

$$\text{NO conversion}\,(\%) = \frac{NO_{inlet} - (NO_{outlet} + NO_{2\ outlet} + N_2O_{outlet})}{NO_{inlet}} \times 100\,(\%) \quad (1)$$

$$NH_3\ \text{conversion}\,(\%) = \frac{NH_{3\,inlet} - NH_{3\,outlet}}{NH_{3\,inlet}} \times 100\,(\%) \quad (2)$$

2.3. Catalyst characterization

The XRD patterns were acquired using X'Pert Pro diffractometer operating at 40 kV and 40 mA with nickel-filtered Cu Kα radiation (λ = 1.5418 Å) in the range $5° < 2\theta < 50°$ with a step size of 0.02°.

Scanning electron microscopy (SEM) image of the samples was measured on a HITACHI S4800 field emission microscope. The samples were pasted on a sample holder using a carbon tape and then covered with Pt film to become conductive. SEM images were taken at magnifications of 10^4 for $Cu_{0.769}/Si_{0.130}Al_{0.435}$ and $Cu_{1.264}/Si_{0.374}Al_{0.441}$ while 5000 for $Cu_{1.122}/Si_{0.106}Al_{0.532}$ with the 5 kV electron beam.

Nuclear magnetic resonance (NMR) experiments were performed on a Varian Infinity plus 300WB spectrometer at resonance frequencies of 121.4, 78.13 and 70 MHz for ^{31}P, ^{27}Al and ^{29}Si nuclei, respectively. The ^{31}P and ^{27}Al MAS NMR spectra were recorded with a spinning rate of 8 kHz while the ^{29}Si MAS NMR spectra were obtained with 5 kHz. The ^{29}Si NMR experiments were only conducted on the aged Cu/SAPO-34 sample. In addition, the quantitative analysis about contents of Si coordination structures was performed by deconvoluting ^{29}Si resonance peaks.

The electron paramagnetic resonance (EPR) spectra were recorded on a Bruker ESP320 spectrometer. The Bruker ESP320E software and the special Bruker program were used for data analysis. Firstly, the EPR spectra were recorded at room temperature and atmospheric pressure. In order to see the hyperfine structure of Cu^{2+} species, dehydration of the samples was carried out prior to EPR experiments. The Cu/SAPO-34 catalysts were evacuated to 4.0×10^{-4} Pa for 8 h at room temperature, and then the sample was heated to 420 °C in the vacuum for another 4 h at the same temperature. After EPR experiments, the dehydrated samples were exposed to air and the EPR spectra were recorded again at room temperature and atmospheric pressure.

Temperature programmed reduction (TPR) experiments were performed in a U-shaped tubular quartz reactor. Prior to reduction, the samples (100 mg) were first treated at 500 °C under a flow of 30 ml/min 2% O_2/N_2 and kept for 30 min. Then, the samples were cooled down to room temperature following by purging in N_2 with a flow of 30 ml/min. In the temperature programmed reduction process, the samples were heated to 900 °C at a ramping rate of 5 °C/min under a flow of 12 ml/min 5% H_2/N_2. The consumption of hydrogen was monitored by a thermal conductivity detector.

Temperature programmed desorption (TPD) experiments were performed in the same reactor for the TPR experiments. Prior to the experiments, the catalysts were pretreated at 500 °C for 10 min in 5 vol.% O_2, and then cooled to 50 °C in N_2. The catalysts were purged by 500 ppm NH_3/N_2 for 40 min or until the outlet NH_3 concentration was stable. The catalysts were purged with N_2 to remove any weakly absorbed NH_3 at 50 °C. When NH_3 concentration was lower than 15 ppm, the catalysts were heated from 50 °C to 550 °C at a ramping rate of 10 °C/min.

3. Results

3.1. XRD and SEM

The XRD patterns show that all HSAPO-34 supports and Cu/SAPO-34 catalysts have the CHA structure. The SEM images demonstrate that all samples own the uniform cubic-like crystals and the crystal sizes of $Si_{0.130}Al_{0.435}$, $Si_{0.374}Al_{0.441}$ and $Si_{0.106}Al_{0.532}$ are 1.0–2.5 μm, 1.5–2.5 μm and 3–5 μm, respectively [9–11]. Moreover, the XRD patterns and SEM images indicate that the loading of Cu does not change the structure of SAPO-34, and the hydrothermal treatment also does not destroy the structure of Cu/SAPO-34 catalysts. The XRD peaks intensities of Cu/SAPO-34 samples calcined at 550 °C increase which is mainly due to the improvement of the crystallinity degree of catalysts after

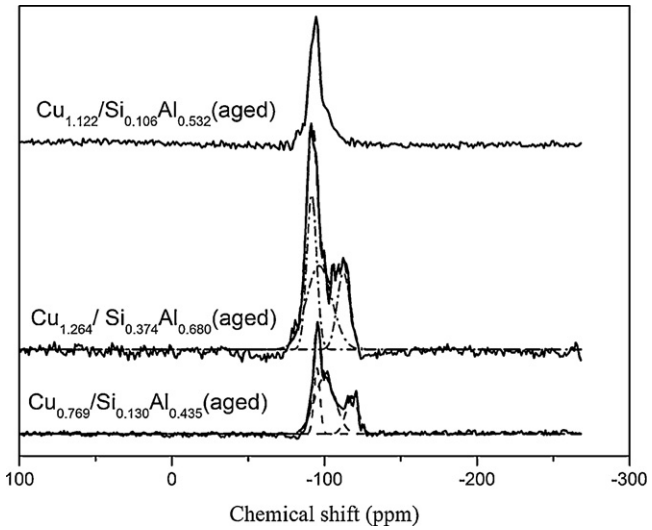

Fig. 1. ^{29}Si NMR spectra of Cu/SAPO-34 catalysts.

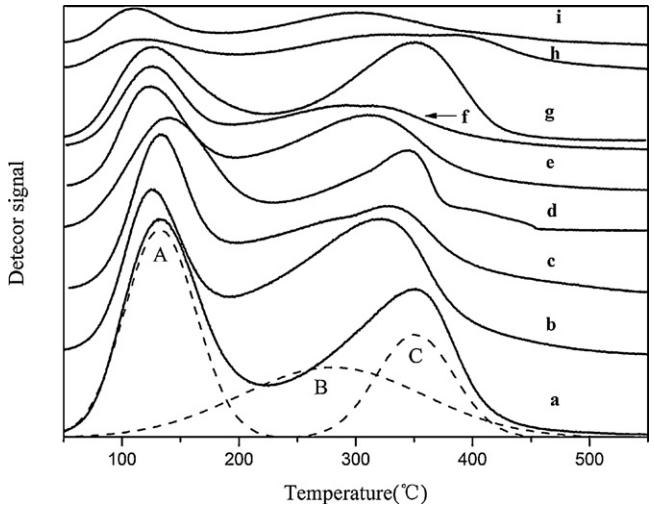

Fig. 2. NH_3-TPD results of all HSAPO-34 and Cu/SAPO-34: (a) $Si_{0.374}Al_{0.441}$; (b) the fresh $Cu_{1.264}/Si_{0.374}Al_{0.441}$; (c) the aged $Cu_{1.264}/Si_{0.374}Al_{0.441}$; (d) $Si_{0.130}Al_{0.435}$; (e) the fresh $Cu_{0.769}/Si_{0.130}Al_{0.435}$; (f) the aged $Cu_{0.769}/Si_{0.130}Al_{0.435}$; (g) $Si_{0.106}Al_{0.532}$; (h) the fresh $Cu_{1.122}/Si_{0.106}Al_{0.532}$; (i) the aged $Cu_{1.122}/Si_{0.106}Al_{0.532}$; NH_3 adsorbed until the NH_3 value was stable. The NH_3-TPD experiment was ramped from 50 °C to 550 °C at a rate of 10 °C/min.

calcinations. The introduction of Cu ions into the supports, decreasing their crystal defects, increases the crystallinity of catalysts [12–15]. Furthermore, there are no peaks related to CuO, Cu_2O species in the XRD, suggesting that the Cu species highly disperse or the formed Cu^{2+} complex is not big enough to be detected. SEM images suggest that the $Si_{0.130}Al_{0.435}$ support has the smallest particle size which may be due to the most structure defects affected by the existence of Si islands [16]. The detailed XRD results and SEM images are listed in Supplementary information.

3.2. NMR

The ^{31}P NMR spectra of the Cu/SAPO-34 catalysts show that there is a single resonance peak around −30.0 ppm for all the catalysts. The peak at −30.0 ppm is assigned to the P (4Al) coordination structure [9–11,17]. The ^{27}Al NMR spectra also show only one resonance peak for all samples, but the peak shifts from 26.5 ppm to 35.3 ppm due to the different number of Si atoms around the Al atoms in Cu/SAPO-34 and this peak represents the Al (4P) framework structure [9–11,17]. Furthermore, each aged catalyst shows no difference in ^{31}P, ^{27}Al NMR spectra compared to the fresh samples, indicating the Cu/SAPO-34 catalysts have excellent hydrothermal structure stability. The detailed ^{31}P and ^{27}Al NMR spectra are listed in Supplementary information.

The ^{29}Si NMR spectra (Fig. 1) show different peaks due to the different Si contents of Cu/SAPO-34 catalysts. Generally, the peak at −90.8 ppm represents the Si (4OAl) structure [9–11,17,18], which can be observed in all SAPO-34 and Cu/SAPO-34 samples. For the $Cu_{1.122}/Si_{0.106}Al_{0.532}$ sample, the ^{29}Si NMR spectrum only appears one resonance peak at −90.8 ppm, which means only Si (4OAl) coordination structure exists in the $Cu_{1.122}/Si_{0.106}Al_{0.532}$ sample [10,18]. There are two peaks at −100.8 ppm and −115.6 ppm over $Cu_{0.769}/Si_{0.130}Al_{0.435}$, which is induced by the Si (2OAl) and the Si (0OAl) coordination structure, respectively [10,18]. The ^{29}Si NMR spectrum of the $Cu_{1.264}/Si_{0.374}Al_{0.441}$ shows the peak at −96.4 ppm and −115.6 ppm, which is ascribed to the Si (3OAl) and the Si (0OAl) coordination structure, respectively [10,18]. The Si (*n*OAl, *n* = 0–3) structures imply the SM3 substitution (Si replaces P and Al) mechanism happens during SAPO-34 synthesis, and this may lead to the formation of Si island [10,19]. The formation of Si islands affects the acidity of the HSAPO-34 supports, because the Si (0OAl) structures in Si islands cannot generate acid site [10,19].

3.3. NH_3-TPD

NH_3-TPD is frequently used to determine the number and strength of the acid sites in catalysts. The NH_3-TPD profiles of HSAPO-34 supports, fresh and aged Cu/SAPO-34 catalysts are shown in Fig. 2. There are two distinct regions at 130–160 °C and 330–360 °C, respectively, for all the catalysts and the two regions can be deconvoluted into three peaks due to the asymmetry of the second peak (A, B and C) [20,21]. The diffuse reflectance infrared Fourier transform spectra (DRIFTS) using NH_3 over samples were performed to ascribe the acid sites (shown in Supplementary information). For the SAPO-34 supports the peak (A) arises at the lower temperature related to the weak Brønsted acid sites at surface hydroxyls. The two peaks (B and C) at the higher temperature are possibly assigned to the structural Brønsted acid sites referred to moderate and strong acidity [16,18,20–24]. In addition, compared to the support the difference of acidic ascription over Cu/SAPO-34 samples is the peaks A and C. The peak A of Cu/SAPO-34 samples represents the adsorbed NH_3 molecules at weak Brønsted acid sites and weak Lewis acid sites related to Cu species and the peak C stands for the adsorbed NH_3 molecules both at strong Brønsted acid sites as SAPO-34 supports and new Lewis acid sites created by the Cu species [24]. The acidity of HSAPO-34 originates from the proton for compensating the unbalanced electronic charges due to Si incorporation into the neutral framework of AlPOs molecular sieves [10,19]. The more Si substitutes, the more acidity sites could form. The TPD results show that the $Si_{0.374}Al_{0.441}$ support, which has the highest Si concentration, has the most acid sites. Table 2 shows the number of acid sites calculated from the NH_3-TPD results. The number of acid sites in $Si_{0.106}Al_{0.532}$ support is more than that of $Si_{0.130}Al_{0.435}$ support, although the Si contents in $Si_{0.106}Al_{0.532}$ support is lower. The main reason for this controversy is due to the formation of Si islands in $Si_{0.130}Al_{0.435}$. Fig. 2 also shows the loading of Cu can decrease the acid sites of HSAPO-34, because the Cu^{2+} species substitute the proton (—Si—OH—Al—) of HSAPO-34 supports [25,26]. And especially for fresh $Cu_{1.122}/Si_{0.106}Al_{0.532}$ sample the number of acid sites decreases almost 52.7% comparing with the $Si_{0.106}Al_{0.532}$ support. The acid strength of the different Si (*n*OAl) (*n* = 1–4) structures is listed as follows: Si (4OAl) < Si (3OAl) < Si (2OAl) < Si (1OAl) [10,19]. The $Cu_{1.122}/Si_{0.106}Al_{0.532}$ sample only has the Si (4OAl) structures, so the amount of adsorbed NH_3 decreased

Table 2
Acidity of the samples obtained from NH_3-TPD.

Sample	Acidity (mmol/g)			Amount
	Weak	Moderate	Strong	
$Si_{0.130}Al_{0.435}$	0.0326	0.0300	0.0090	0.0715
$Cu_{0.769}/Si_{0.130}Al_{0.435}$ (fresh)	0.0253	0.0156	0.0252	0.0662
$Cu_{0.769}/Si_{0.130}Al_{0.435}$ (aged)	0.0193	0.0074	0.0195	0.0462
$Si_{0.374}Al_{0.441}$	0.0520	0.0518	0.0286	0.1323
$Cu_{1.264}/Si_{0.374}Al_{0.441}$ (fresh)	0.0357	0.0361	0.0415	0.1133
$Cu_{1.264}/Si_{0.374}Al_{0.441}$ (aged)	0.0315	0.0262	0.0309	0.0887
$Si_{0.106}Al_{0.532}$	0.0246	0.0196	0.0285	0.0726
$Cu_{1.122}/Si_{0.106}Al_{0.532}$ (fresh)	0.0089	0.0082	0.0173	0.0343
$Cu_{1.122}/Si_{0.106}Al_{0.532}$ (aged)	0.0080	0.0067	0.0130	0.0277

significantly compared to other samples. The Cu/SAPO-34 catalysts with various Si contents show different strengths and the number of acid sites, and the fresh $Cu_{1.264}/Si_{0.374}Al_{0.441}$ catalyst has the highest acidic content among three catalysts.

3.4. H_2-TPR

Fig. 3 presents the H_2-TPR results of three Cu/SAPO-34 catalysts. The H_2 consumption peak from 200 °C to 600 °C can be divided into three peaks after deconvolution and curve stochastic fitting procedures by Lorentzian method, and the TPR curve of HSAPO-34 was subtracted as the baseline of the Cu/SAPO-34 sample. The peak at the lower temperature (peak A) represents the reduction of isolated Cu^{2+} to Cu^+ [27–33], the moderate one (peak B) represents the reduction of the bulk copper oxide in zeolites from CuO to Cu^0 [31,33,34], and the third one (peak C) at the higher temperature comes from the reduction from Cu^+ to Cu^0 [27–33]. This H_2 consumption peak can be assigned to the reduction of "L (Low)-Cu^+", including the one obtained from the reduction of isolated Cu^{2+} and the original Cu^+ existed on the framework of SAPO-34. Another H_2 consumption peak above 700 °C (peak D) can be attributed to the reduction of highly stable Cu^+ to Cu^0 [31–33,35,36], which is named as "H (High)-Cu^+". Bulánek [37] and Torre [32,33] found that the reducibility of Cu species in Cu-zeolites can be changed in a wide range by the coordination to zeolite framework oxygen. The more Al existed in the zeolites can cause higher negative charge of the zeolites, which strengthened the ligand of Cu species to the matrix. So the H_2 consumption peaks, reduction of Cu^+ to Cu^0 in

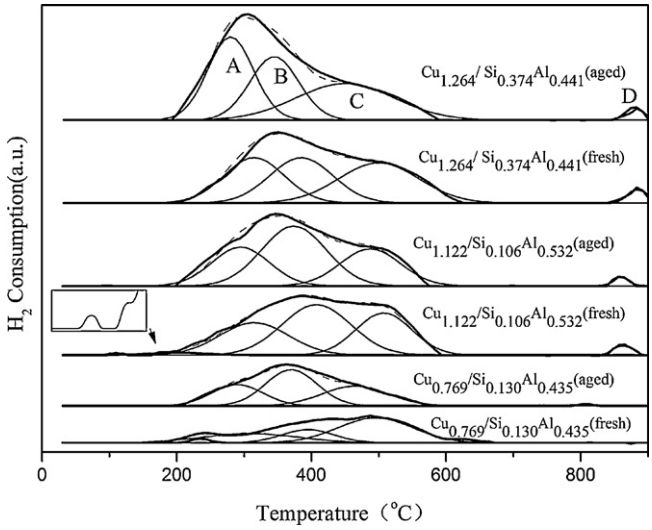

Fig. 3. H_2-TPR results of all Cu/SAPO-34 catalysts. The feed containing was 5 vol.% H_2 in N_2 and fed at a flow rate of 12 cm^3/min and the experiment was performed from 30 °C to 900 °C with the heating up rate of 5 °C/min.

Table 3
Temperatures related with the TPR profiles of the catalysts.

Sample	Temperature (°C)				
	CuO cluster	A	B	C	D
$Cu_{0.769}/Si_{0.130}Al_{0.435}$ (fresh)	235	310	395	495	0
$Cu_{0.769}/Si_{0.130}Al_{0.435}$ (aged)	–	290	370	465	805
$Cu_{1.264}/Si_{0.374}Al_{0.441}$ (fresh)	–	315	385	500	885
$Cu_{1.264}/Si_{0.374}Al_{0.441}$ (aged)	–	280	345	450	880
$Cu_{1.122}/Si_{0.106}Al_{0.532}$ (fresh)	110/200	315	408	508	863
$Cu_{1.122}/Si_{0.106}Al_{0.532}$ (aged)	–	280	374	487	860

Cu-zeolites, were above 800 °C. Richter [36] found that the Cu^+ species were reduced at 525 °C and 770 °C, and the H_2 consumption at the higher temperature was due to the formation of stable Cu^+ species in Cu-zeolites. It is deduced that the H (High)-Cu^+ coordinated to framework oxygen is more stable and more difficult to be reduced for the higher negative charge of zeolites. Moreover, the fresh $Cu_{1.122}/Si_{0.106}Al_{0.532}$ exhibits peaks at 110 °C, 220 °C and $Cu_{0.769}/Si_{0.130}Al_{0.435}$ exhibits peak at 235 °C, which are due to the reduction of surface CuO cluster to Cu^0 [29,30,32,33,36].

The loading and environment of Cu^{2+} species are different due to the different Si contents of the three SAPO-34 supports, which results in different reducibility of Cu^{2+} species in three Cu/SAPO-34 catalysts. It has been reported that the compositions of the support and the Cu loading affected the reduction temperature of Cu species in molecular sieves [32–34,37,38]. As shown in Table 3, the reduction peaks (A, B, and C) of the fresh $Cu_{1.122}/Si_{0.106}Al_{0.532}$ sample are higher than others, suggesting that the reducibility of the $Cu_{1.122}/Si_{0.106}Al_{0.532}$ sample is lower. One possible reason is the highest Al content in $Cu_{1.122}/Si_{0.106}Al_{0.532}$ sample. Because the AlO_4 in SAPO-34 displays negative charge, the ligand strength of Cu species to the skeletal oxygen atoms in the $Cu_{1.122}/Si_{0.106}Al_{0.532}$ sample may be stronger than that in other samples, which cause the lower reducibility of the Cu species [32–34].

3.5. EPR

EPR spectra can characterize the hyperfine structure of Cu^{2+} species and Figs. 4 and 5 show the EPR spectra of the fresh and aged Cu/SAPO-34 catalysts performed at room temperature, respectively. The Cu^{2+} species loaded in Cu/SAPO-34 samples display axial symmetry for all spectra. For the fresh Cu/SAPO-34, one peak, which is characteristic of the hydrated Cu^{2+} species in site

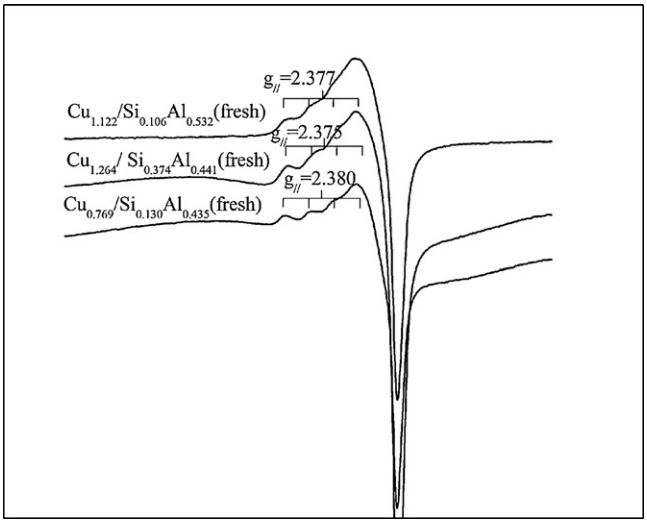

Fig. 4. EPR spectra of the fresh Cu/SAPO-34 catalysts at room temperature and atmospheric pressure.

Table 4
EPR parameters of all Cu/SAPO-34 after different treatments.

Sample	Normal temperature and pressure		Vacuum and high temperature				Exposed to air again	
	$g_{\parallel}$	A	Cu^{2+} (I)		Cu^{2+} (III)		$g_{\parallel}$	A
			$g_{1\parallel}$	A_1	$g_{2\parallel}$	A_2		
$Cu_{0.769}/Si_{0.130}Al_{0.435}$ (fresh)	2.380	121.57	2.392	102.28	2.352	114.62	2.380	128.92
$Cu_{0.769}/Si_{0.130}Al_{0.435}$ (aged)	2.379	118.77	2.393	106.31	2.344	119.36	2.382	121.45
$Cu_{1.264}/Si_{0.374}Al_{0.441}$ (fresh)	2.375	118.54	2.392	106.56	2.355	112.82	2.389	105.09
$Cu_{1.264}/Si_{0.374}Al_{0.441}$ (aged)	2.387	107.04	2.393	107.44	2.359	109.35	2.392	101.92
$Cu_{1.122}/Si_{0.106}Al_{0.532}$ (fresh)	2.377	124.70	2.392	104.52	2.349	118.77	2.387	111.03
$Cu_{1.122}/Si_{0.106}Al_{0.532}$ (aged)	2.384	118.87	2.392	105.83	2.336	127.31	2.374	120.42

(I) (Cu^{2+} (I)) [25,26], is observed with EPR parameters shown in Table 4. In Fig. 5 the aged Cu/SAPO-34 samples also show the characteristic peak for Cu^{2+} species in site (I) [25,26]. Kevan [25,26] suggested that Cu^{2+} species can be located at four sites in Cu/SAPO-34 framework and the Cu^{2+} species in different sites showed various EPR parameters. It had been observed that the Cu^{2+} species on different locations can migrate upon different treatments. Here, the aged $Cu_{1.122}/Si_{0.106}Al_{0.532}$ catalyst is set as an example to study the migration of the Cu^{2+} species in zeolites. For the aged $Cu_{1.122}/Si_{0.106}Al_{0.532}$ sample, Cu^{2+} (I) species are observed with EPR parameters of $g_{\parallel} = 2.384$ and $A_{\parallel} = 118.87\ cm^{-1}$ based on spectrum A in Fig. 6. After dehydration at 420 °C, two axially symmetric signals appear and superimpose in Fig. 6B. The dominant signal with $g_{\parallel} = 2.392$ and $A_{\parallel} = 105.83\ cm^{-1}$ is ascribed to the Cu^{2+} (I) complex, while the other signal with $g_{\parallel} = 2.336$ and $A_{\parallel} = 127.31\ cm^{-1}$ is assigned to the Cu^{2+} complex in site (III) (Cu^{2+} (III)) [25,26]. When the dehydrated aged $Cu_{1.122}/Si_{0.106}Al_{0.532}$ is exposed to air again, only one EPR signal with $g_{\parallel} = 2.374$ and $A_{\parallel} = 120.42\ cm^{-1}$ is observed, indicating only the Cu^{2+} (I) species exist in Fig. 6C. The detailed EPR spectra of all Cu/SAPO-34 samples after dehydration and exposed to air again are listed in Supplementary information.

According to the EPR parameters of Cu/SAPO-34 catalysts summarized in Table 4, all the Cu/SAPO-34 catalysts show the same changes of Cu^{2+} complex after different treatments, and only one type of Cu^{2+} (I) species is observed in the hydrated sample. The $g_{\parallel}$ value and hyperfine coupling constant for Cu^{2+} complex in each Cu/SAPO-34 are different, which is possibly due to the different Si and Al contents in the support, influencing the banding force between the Cu species and the framework of the support and probably causing the distortion for the Cu^{2+} location [39,40].

The EPR parameters of the hydrated sample are characteristic of an octahedrally coordinated Cu^{2+} complex, coordinated to three water molecules [25,26]. In Fig. 6A, the hydrothermal aged $Cu_{1.122}/Si_{0.106}Al_{0.532}$ catalyst presents one peak ascribed to the Cu^{2+} species in site (I) as mentioned above. Upon evacuation at 420 °C, two cupric species are observed, since it is sufficient to remove water ligands under this condition. After the removal of the absorbed H_2O, the EPR spectrum of the aged $Cu_{1.122}/Si_{0.106}Al_{0.532}$ catalyst shows two hyperfine structures of Cu^{2+} species in Fig. 6B. The parameters in Table 4 show that the Cu^{2+} species giving rise to $g_{\parallel} = 2.392$ represents the Cu^{2+} complex in site (I), in which the Cu^{2+} is octahedrally coordinated to three framework oxygen and three water molecules. The site (I) is displaced from the six-ring into the ellipsoidal cavity [25]. Meanwhile, the Cu^{2+} species with $g_{\parallel} = 2.336$ represents the Cu^{2+} complex in site (III) over Cu/SAPO-34 sample, which locate in the center of the hexagonal prism [25]. When the dehydrated sample is exposed to air again, the Cu^{2+} complex coordinates with water molecules again as the Cu^{2+} complex in the hydrated sample and the two hyperfine structures of Cu^{2+} species disappear, which is similar to the EPR spectra of Fig. 6A. The appearance of another type of Cu^{2+} species after dehydration indicates the existence of at least two different Cu sites in the Cu/SAPO-34 catalysts and Cu^{2+} species could migrate from one to another upon pretreatment [25,26,41]. It also can be concluded that the absorbed H_2O molecules change the coordination of Cu^{2+} complex of the catalysts and the dehydration process is reversible [25,26].

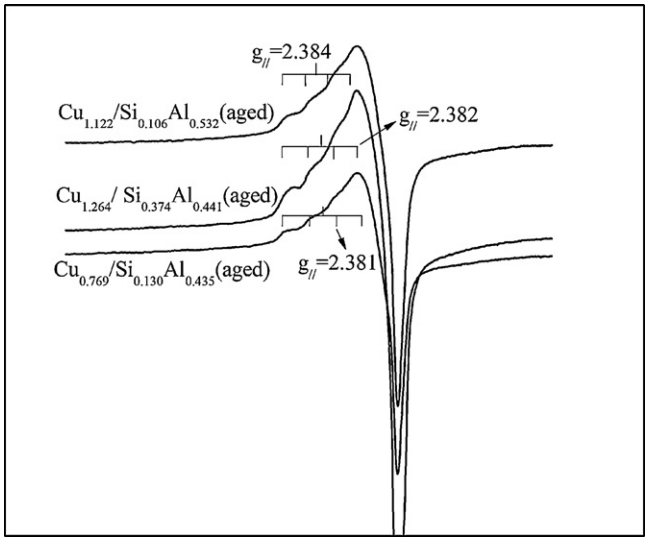

Fig. 5. EPR spectra of the aged Cu/SAPO-34 catalysts at room temperature and atmospheric pressure.

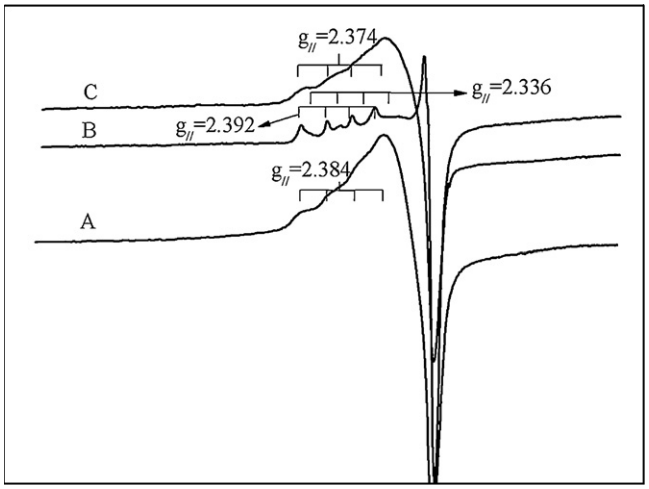

Fig. 6. EPR spectra of the aged $Cu_{1.122}/Si_{0.106}Al_{0.532}$ catalysts: (A) the EPR spectra at room temperature and pressure; (B) the EPR spectra after vacuum and heat treatment. The condition is that: the catalysts were vacuumized at 4.0×10^{-4} Pa for 8 h at room temperature, then rose the temperature to 420 °C and kept evacuation 4 h at this temperature. (C) The EPR spectra were exposed to air after the vacuum.

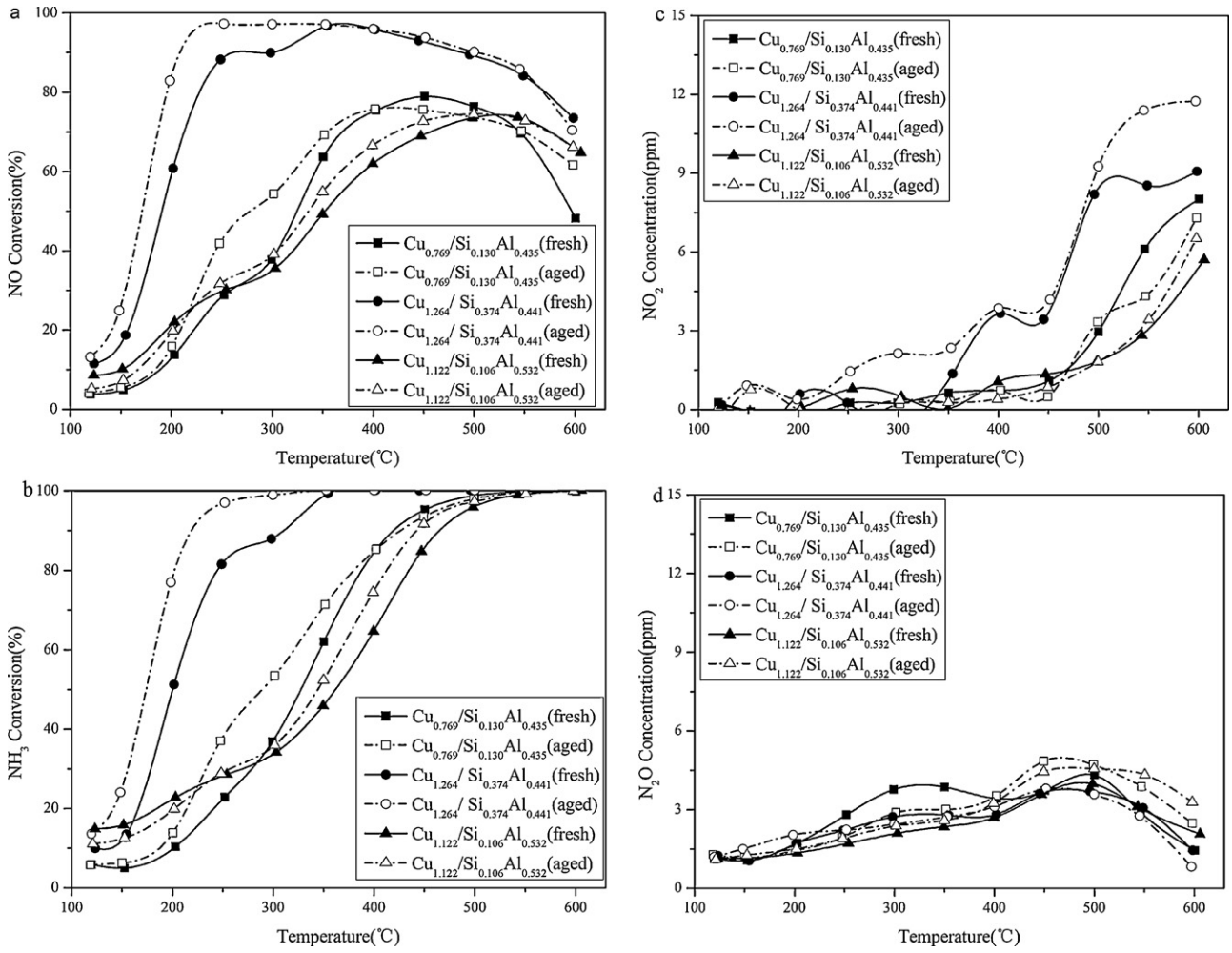

Fig. 7. Catalytic performance of the fresh (aged) $Cu_{0.769}/Si_{0.130}Al_{0.435}$, $Cu_{1.122}/Si_{0.106}Al_{0.532}$, $Cu_{1.264}/Si_{0.374}Al_{0.441}$ catalysts as a function of temperature during the NH_3-SCR process: (a) NO conversion; (b) NH_3 conversion; (c) NO_2 generation and (d) N_2O generation. The feed contains 500 ppm NH_3, 500 ppm NO, 5% O_2, N_2 is the balance. The flow rate and the space velocity in all experiment were controlled at 1000 ml/min and 35,000 h^{-1}.

3.6. Catalyst activity

NH_3-SCR performance of various catalysts is shown in Fig. 7a as a function of temperature. For the fresh $Cu_{1.264}/Si_{0.374}Al_{0.441}$ catalyst, the NO conversion above 80% is achieved between 230 °C and 560 °C. The NO conversion over the fresh $Cu_{1.264}/Si_{0.374}Al_{0.441}$ sample is higher than other fresh samples in tested temperature range (120–600 °C), and the fresh $Cu_{1.122}/Si_{0.106}Al_{0.532}$ sample and fresh $Cu_{0.769}/Si_{0.130}Al_{0.435}$ samples have similar NO conversion. After the hydrothermal treatment at 750 °C for 12 h, all the aged Cu/SAPO-34 catalysts maintain their SCR activity, suggesting that Cu/SAPO-34 catalysts have excellent hydrothermal stability.

The NH_3 conversions during the NH_3-SCR process are shown in Fig. 7b. Generally, the NH_3 conversions increase with the increasing temperature. The $Cu_{1.264}/Si_{0.374}Al_{0.441}$ catalyst shows the highest NH_3 conversion. Furthermore, compared with the fresh samples, NH_3 conversion on the aged samples shows the similar trend to that of the NO conversion. Fig. 7c and d shows that the NO_2 and N_2O concentrations are below 12 ppm and 5 ppm, respectively. In addition, the SCR performance with H_2O shown in Fig. 8 presents that the H_2O does not strongly influence the activity of Cu/SAPO-34 catalysts.

4. Discussion

4.1. The effect of Si content on the structure of Cu/SAPO-34 catalysts

According to the chemical composition shown in Table 1 and the structure characterization of catalysts, it is concluded that the Si content can directly affect the structure of Cu/SAPO-34 catalysts. Firstly, the Si content can affect the crystal size of SAPO-34 supports. $Si_{0.106}Al_{0.532}$ (3–5 μm) shows the biggest crystal size for the highest degree of crystallinity. Due to the formation of Si islands in SAPO-34, it will influence silicon distribution and change both the involved angle and the length of TOT (T stands for Al, Si, P atoms placing in the center of the tetrahedron) band that affect the crystallinity of SAPO-34 [16]. The $Si_{0.130}Al_{0.435}$ support (1.0–2.5 μm) has a smaller crystal size, because the deviation of the TOT band length and angle is limited by the presence of Si islands. While crystal sizes among three supports was not obvious, this may be due to the lower amount of Si islands formed in the $Si_{0.374}Al_{0.441}$ and $Si_{0.130}Al_{0.435}$ supports.

If the mole ratio of the (Si + P)/Al equals to 1, Si atom substitutes P and forms the Si (4OAl) species. If the mole ratio of (Si + P)/Al is bigger than 1, both the Si atom substitution P and Al occur [10].

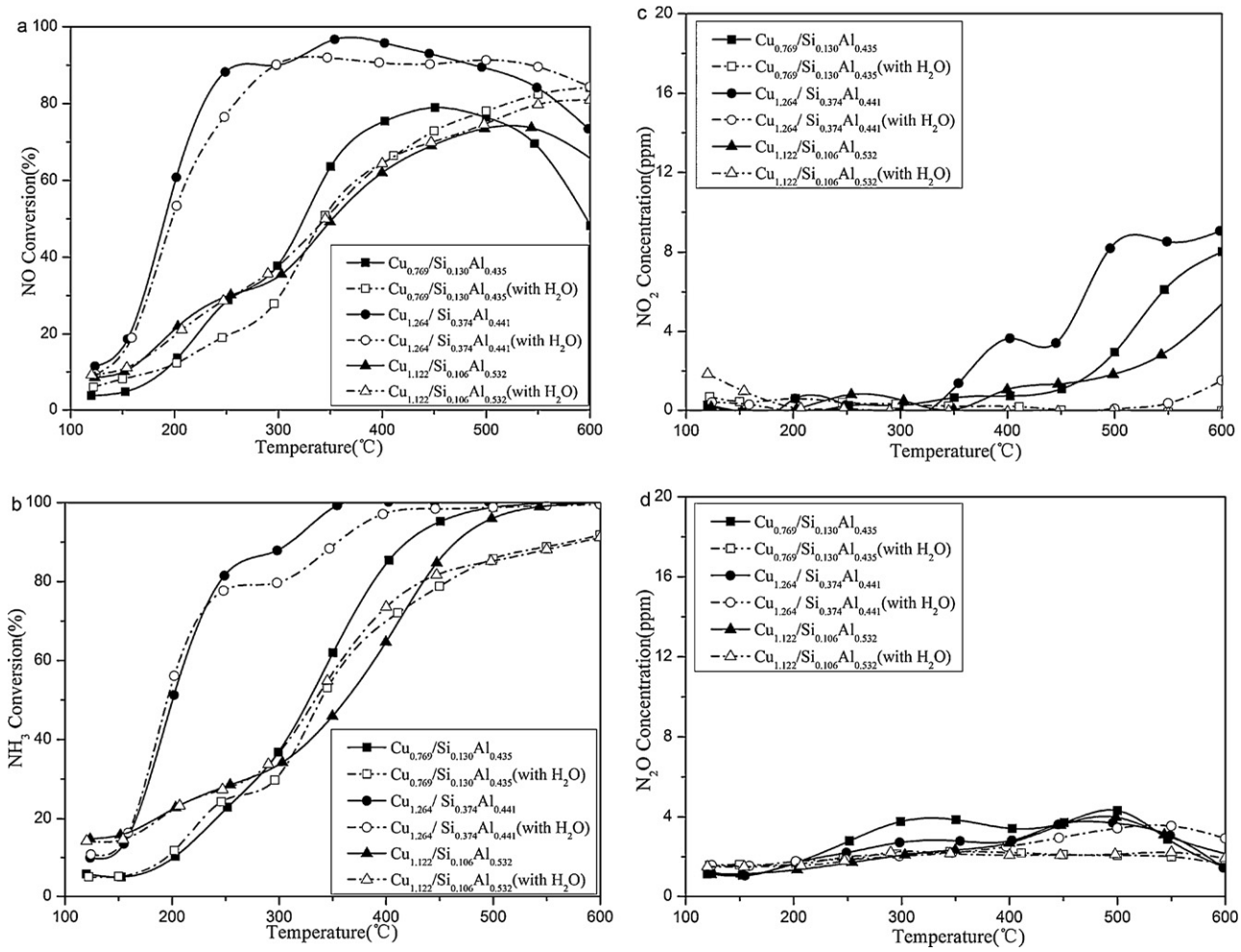

Fig. 8. (a) The NO conversion, (b) the NH_3 conversion, (c) NO_2 concentrations, (d) N_2O concentrations from activity test over fresh Cu/SAPO-34 catalysts with H_2O in the inlet gas. The feed contains 500 ppm NH_3, 500 ppm NO, 5% O_2, N_2 is the balance. The 5% H_2O content was added in the test to evaluate the effect of H_2O to the activity. The flow rate and the space velocity in all experiment were controlled at 1000 ml/min and 35,000 h^{-1}.

As presented in Table 1, the (Si + P)/Al ratios of $Cu_{0.769}/Si_{0.130}Al_{0.435}$ and $Cu_{1.264}/Si_{0.374}Al_{0.441}$ samples are bigger than 1, so Si islands exist in both of them. The ^{29}Si NMR spectra in Fig. 1 suggest only Si (4OAl) structure exists in the aged $Cu_{1.122}/Si_{0.106}Al_{0.532}$ sample. However, Si islands and Si (*n*OAl) (*n* = 0–4) coordination structures exist in the aged $Cu_{0.769}/Si_{0.130}Al_{0.435}$ and $Cu_{1.264}/Si_{0.374}Al_{0.441}$ samples. Table 5 presents the different Si coordination structures and their contents in the Cu/SAPO-34 samples. It can be seen that the $Cu_{1.264}/Si_{0.374}Al_{0.441}$ sample has less Si (0OAl) structures than the $Cu_{0.769}/Si_{0.130}Al_{0.435}$ sample. The acidity of Cu/SAPO-34 sample comes from the substitution of P by Si [10,19]. The Si (*n*OAl) (*n* = 1–4) structures in $Si_{0.374}Al_{0.441}$ support are much more than that in other supports, which mean that number of acid sites in $Cu_{1.264}/Si_{0.374}Al_{0.441}$ is the most among the Cu/SAPO-34 samples. Furthermore, the $Si_{0.130}Al_{0.435}$ support shows less acid sites than the $Si_{0.106}Al_{0.532}$ support due to the formation of Si islands, which cannot generate the acid sites. Table 5 shows that the $Si_{0.130}Al_{0.435}$ support has less Si (*n*OAl) (*n* = 1–4) structures than that of the $Si_{0.106}Al_{0.532}$ support. In other words, the number of Si atoms generating acid sites in $Si_{0.106}Al_{0.532}$ is bigger than that of $Si_{0.130}Al_{0.435}$ supports.

Table 5
Distribution (%) of silicon environments from silicon MAS NMR spectra.

Sample	Si(4OAl)	Si(3OAl)	Si(2OAl)	Si(0OAl)
$Cu_{0.769}/Si_{0.130}Al_{0.435}$	19.5	0	58.5	22.0
$Cu_{1.264}/Si_{0.374}Al_{0.441}$	33.0	45.9	0	21.1
$Cu_{1.122}/Si_{0.106}Al_{0.532}$	100	0	0	0

The Cu loading over Cu/SAPO-34 is affected by the supports using the same procedure and the correlation between the amount of Cu loading and the Si and Al content is summarized in Fig. 9. Firstly, the Cu loading depends on both the Si contents and the Al contents of SAPO-34 supports. In Fig. 9a, $Cu_{1.264}/Si_{0.374}Al_{0.441}$ sample possesses higher Cu loading than others. Since Cu can only be located at the acidity sites of SAPO-34 supports originated from the Si substitution in theory, the SAPO-34 support which has higher Si contents is easier for the Cu exchanging. In addition, the AlO_4 structures in the framework of SAPO-34 support display negative charge, which is convenient for the migration of Cu^{2+} species during the exchanging process [39,42,43]. As shown in Fig. 9b, the high Cu loading on the $Cu_{1.122}/Si_{0.106}Al_{0.532}$ is consistent with its higher Al contents, while the lower Cu loading is observed in $Cu_{0.769}/Si_{0.130}Al_{0.435}$ sample related to its lower Al content.

4.2. The effect of Si content on the acidity of Cu/SAPO-34 catalysts

Table 2 shows that the number of acid sites is decided by the Si content, meanwhile the loading of Cu species in SAPO-34 molecular sieves decreases the number of acid sites. Moreover, it seems that the loading of Cu species decrease the weak and moderate acid sites, but the number of strong acid sites increases, indicating

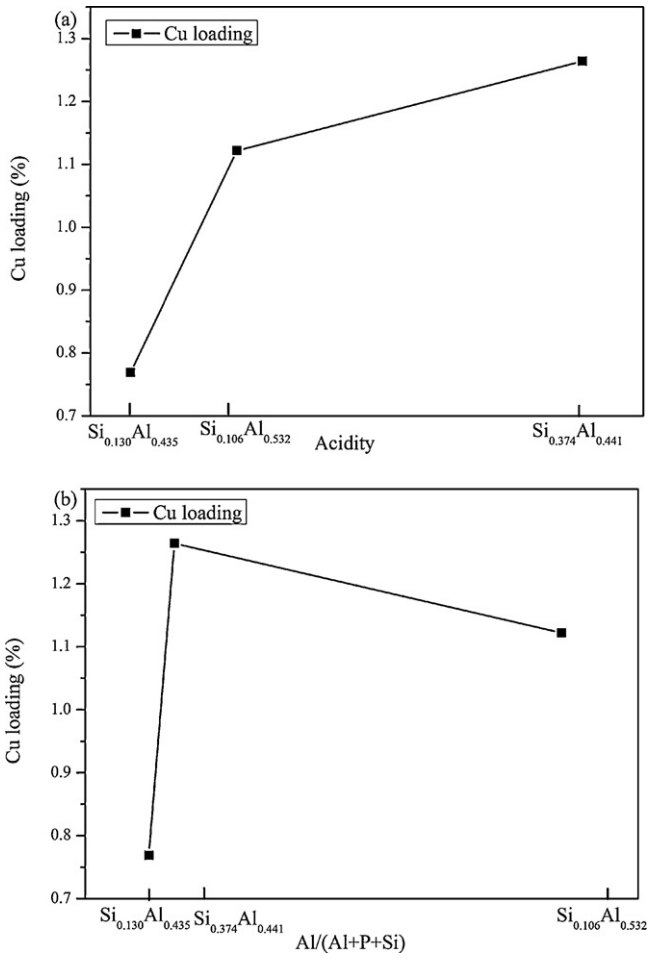

Fig. 9. (a) Relationship between the acidity of SAPO-34 molecular sieves and the Cu loading on zeolites. The acidity originates from integrating the profiles of NH_3-TPD. (b) Relationship between the Al contents and the Cu loading on Cu/SAPO-34 zeolites.

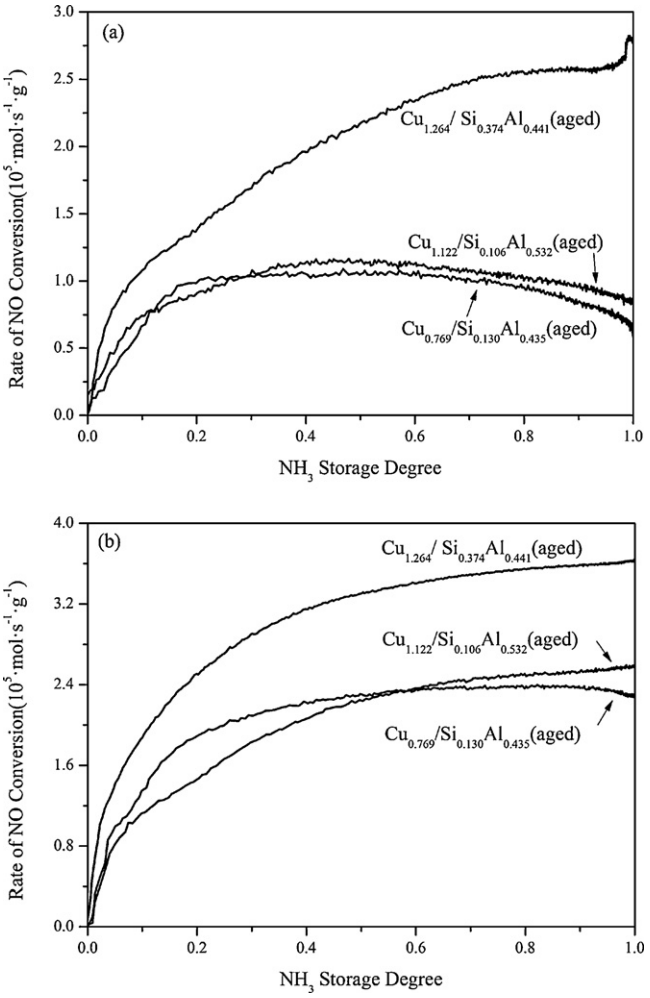

Fig. 10. Relationship between the NH_3 storage and the rate of NO conversion on aged Cu/SAPO-34 samples at (a) 200 °C and (b) 250 °C. Firstly, the inlets of NO 500 ppm, O_2 5 vol.% attained equilibrium, then the NH_3 500 ppm were cut-in and reach steady. The flow rate is 1 L/min and the temperature kept at 200 °C and 250 °C.

that the Cu species, exchanged in Cu/SAPO-34, can generate new strong acid sites [24]. In addition, because the adsorption of NH_3 is the key step in the whole process of SCR reaction [1], the various numbers of acid sites in the Cu/SAPO-34 samples can affect their SCR activities. For example, the $Cu_{1.264}/Si_{0.374}Al_{0.441}$ sample with more number of acid sites performs high NO conversion and the $Cu_{1.122}/Si_{0.106}Al_{0.532}$ sample with less acid contents perform the low NO conversion.

To further investigate the relation between acidity and the SCR activity, the NH_3 adsorption and NO conversion rates on the different aged samples at 200 °C, 250 °C were studied and the results are summarized in Fig. 10. Firstly at 200 °C, the aged $Cu_{1.264}/Si_{0.374}Al_{0.441}$ sample shows the highest rate of NO conversion and the rate increases with the increasing NH_3 storage degree; however, the NH_3 inhibition effect appears on aged $Cu_{0.769}/Si_{0.130}Al_{0.435}$ and $Cu_{1.122}/Si_{0.106}Al_{0.532}$ catalysts and the rate of NO conversion reaches the maximum when the NH_3 storage degree reaches 0.19 and 0.36, respectively. The different NH_3 inhibition effects over various Cu/SAPO-34 samples may be related with the extent of Cu^{2+} ions covered by adsorbed NH_3. The oxidation of NO and formation of surface NO_x adsorption complexes over Cu species in Cu/zeolites are the key elemental step in NH_3-SCR reaction [1]. In addition, it is known that the NH_3 inhibition is due to the adsorption of NH_3 on the active sites, which may interfere with the oxidation of NO and/or the redox properties over SCR catalysts [44,45]. The in suit DRIFTS of NH_3 chemisorption at 200 °C (shown in Supplementary information) presents that three Cu/SAPO-34 catalysts adsorb the same Cu-NH_3 species with similar bands intensity and these acid sites are mainly ascribed to the strong acid sites. Moreover, the amount of NH_3 adsorbed on the strong acid sites over catalysts at 200 °C is shown in Fig. 11b. The three Cu/SAPO-34 samples adsorb the similar contents of NH_3 on strong acid sites though the $Cu_{1.264}/Si_{0.374}Al_{0.441}$ sample owns much more Cu^{2+} ions than that of the other catalysts. It is predicted that the Cu^{2+} ions over the $Cu_{1.264}/Si_{0.374}Al_{0.441}$ sample are not completely covered by NH_3, which could leave enough active Cu^{2+} ions for the oxidation of NO during the reaction [44,45]. Therefore, the NH_3 inhibition was not apparent over $Cu_{1.264}/Si_{0.374}Al_{0.441}$ sample. Fig. 10b shows the same trend on the aged samples at 250 °C and it is seen that the NO conversion is related to the acidic property of Cu/SAPO-34 sample. In addition, Fig. 11a presents the amount of absorbed NH_3 on three aged samples at 200 °C, 250 °C when the SCR reactions attain equilibrium. The number of absorbed NH_3 on Cu/SAPO-34 in Fig. 11a matches the NO conversion in Fig. 7a very well, which means that the more NH_3 molecules the samples adsorb, the higher NO conversion the catalysts own. Fig. 11c and d shows that the NO conversions over Cu/SAPO-34 are mainly related to the adsorption capacity of ammonia on the catalysts. The low SCR activities of $Cu_{1.22}Si_{0.106}Al_{0.532}$ and $Cu_{0.769}Si_{0.130}Al_{0.435}$ samples are related to their low number of acid sites at low temperature. It can be concluded that the NO conversion rate follows the same trend of the order of the NH_3 adsorption capacity on the Cu/SAPO-34

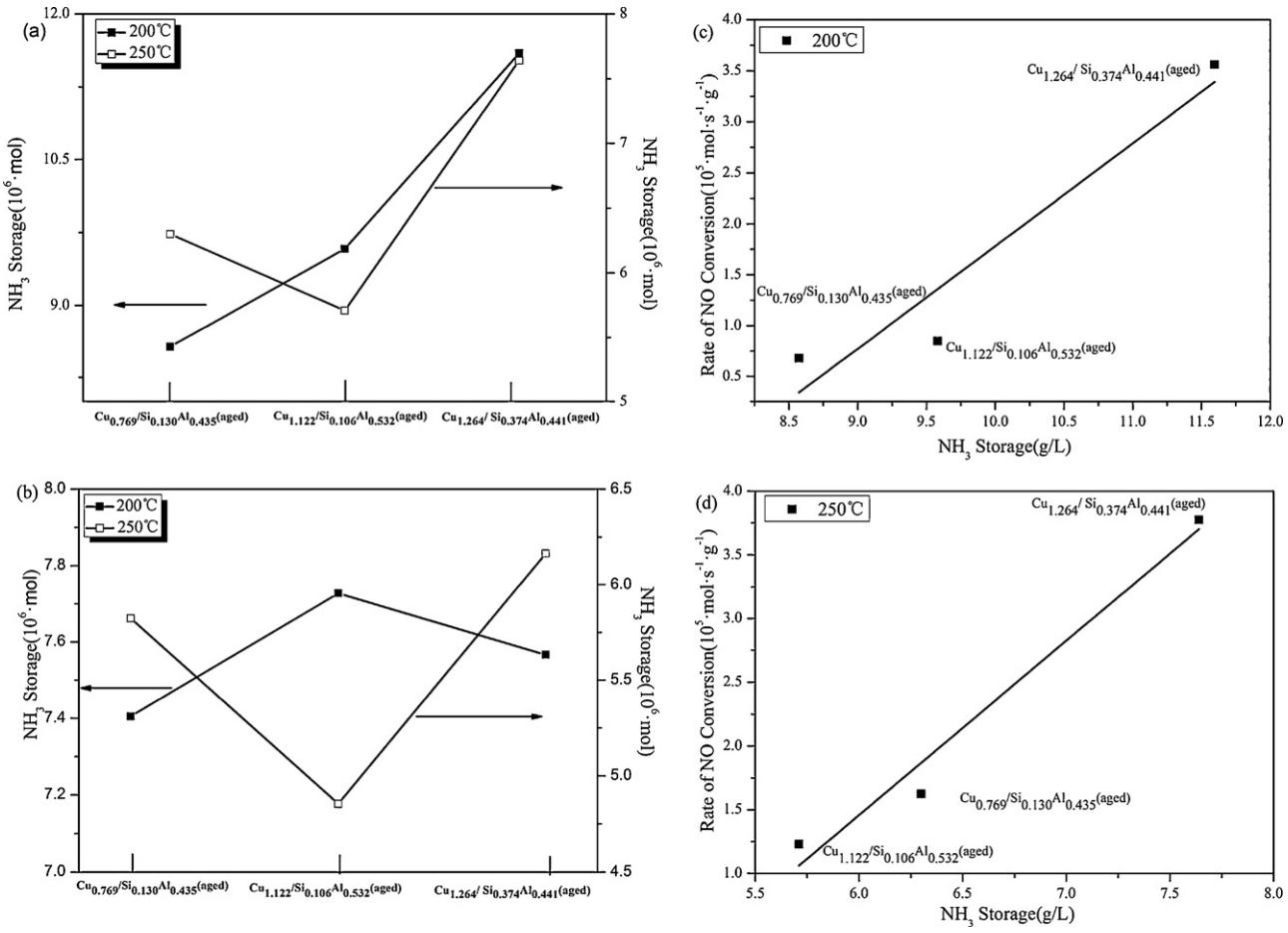

Fig. 11. (a) NH_3 storage on aged samples at 200 °C, 250 °C. (b) the contents of NH_3 adsorbed on the strong acid sites over aged Cu/SAPO-34 catalysts at 200 °C, 250 °C. (c) The relationship between the NH_3 storage and the rate of NO conversion at 200 °C. (d) The relationship between the NH_3 storage and the rate of NO conversion at 250 °C. The experiments conditions: after the SCR equilibrium was attained on samples at 200 °C/250 °C, all of the inlets were cutoff except N_2. Then the NH_3-TPD was performed to estimate the NH_3 storage. The flow rate is 1 L/min and the tests were performed at 200 °C/250 °C, respectively.

catalysts, indicating that the SCR activity over Cu/SAPO-34 are not only related with their content of active sits.

Finally, the acidity of the Cu/SAPO-34 could not be the sole factor to determine SCR activity, for example, the aged $Cu_{1.122}/Si_{0.106}Al_{0.532}$ stores much more NH_3 than that of the aged $Cu_{0.769}/Si_{0.130}Al_{0.435}$ at 200 °C, while the NO conversion is similar on both aged catalysts. So it is deduced that the content of Cu species is also related to the SCR activities of Cu/SAPO-34 samples with various Si contents.

4.3. The effect of Si content on the environment of Cu species in Cu/SAPO-34

The present work demonstrates that the Cu/SAPO-34 samples via the same method have the various contents of Cu species, resulting in significant differences in both SCR activities and structural properties. The outcome of H_2-TPR in Table 6 shows the effect of Si content on the Cu species in Cu/SAPO-34 samples. It can be seen that the $Cu_{1.264}/Si_{0.374}Al_{0.441}$ sample has the most number of isolated Cu^{2+} species which is consistent with the highest number of acid sites in $Si_{0.374}Al_{0.441}$. The SAPO-34 supports with more number of acid sites, related to the Si contents studied above, is propitious to the increment of Cu^{2+} ions in Cu/SAPO-34. In addition, the Al contents also affect the contents of Cu species in Cu/SAPO-34 samples. Though the $Cu_{1.122}/Si_{0.106}Al_{0.532}$ and $Cu_{1.264}/Si_{0.374}Al_{0.441}$ samples have the similar Cu loading, the $Cu_{1.122}/Si_{0.106}Al_{0.532}$ sample owns the more bulk copper oxide in Table 6. And the formation of CuO over $Cu_{1.22}Si_{0.106}Al_{0.532}$ sample is mainly due to the high Al content and the less acid sites [32–34]. If excess Cu^{2+} species migrate to the supports for its higher Al contents without enough acid sites near them, the excess Cu^{2+} species which do not locate on the acid sites may generate bulk copper oxide in the catalysts and/or CuO cluster on the surface of zeolites during the calcination. In addition, the H_2/Cu ratios over samples in Table 6 can also illustrate the valence states of Cu species, and it is seen that the lower H_2/Cu ratios over $Cu_{0.769}/Si_{0.130}Al_{0.435}$ sample resulted from lots of Cu^+ species. Larsen [46,47] also found the high content of Cu^+ species formed in Cu/zeolites after pretreatment due to auto-reduction of Cu^{2+} to Cu^+. The auto-reduction of Cu^{2+} was affected by the nature of the Cu^{2+} location and the Cu^{2+} located near more acid sites would not be expected to undergo the auto-reduction after heat treatment. In $Cu_{0.769}/Si_{0.130}Al_{0.435}$ sample the least number of acid sites may cause the auto-reduction of Cu^{2+} to Cu^+ before H_2-TPR.

Compared with the SAPO-34 support, the existence of Cu species gives Cu/SAPO-34 sample the high SCR activity, and the isolated Cu^{2+} species is proved to be the active sites for NH_3-SCR reaction over Cu chabazite catalysts [7]. In addition, the EPR is inactive for CuO, binuclear species, or Cu^+ ions but active for isolated Cu^{2+} species [48–50]. The contents of isolated Cu^{2+} species from EPR are calculated and summarized in Fig. 12a, and the outcome of H_2-TPR in Table 6 shows the same results of isolated Cu^{2+} species in Cu/SAPO-34 samples. It can be seen that the $Cu_{1.264}/Si_{0.374}Al_{0.441}$ sample has the most content of isolated Cu^{2+} species which is consistent with the highest NO conversion over

Table 6
Contents of different Cu species on Cu/SAPO-34 from the H_2-TPR results.

Sample	Copper species content (μmol/g Cu/SAPO-34)					H_2/Cu (mol/mol)
	Surface CuO cluster	Isolated Cu^{2+}	Bulk copper oxide in cage	Cu^+	Amount	
$Cu_{0.769}/Si_{0.130}Al_{0.435}$ (fresh)	0.283	6.6070	2.596	7.551	17.037	0.580
$Cu_{0.769}/Si_{0.130}Al_{0.435}$ (aged)	0	8.306	7.079	1.793	17.178	0.712
$Cu_{1.264}/Si_{0.374}Al_{0.441}$ (fresh)	0	20.765	10.854	5.582	37.472	0.920
$Cu_{1.264}/Si_{0.374}Al_{0.441}$ (aged)	0	29.071	11.798	0.0001	40.870	1.087
$Cu_{1.122}/Si_{0.106}Al_{0.532}$ (fresh)	0.661	16.990	13.214	2.454	33.319	0.945
$Cu_{1.122}/Si_{0.106}Al_{0.532}$ (aged)	0	17.084	14.724	1.038	32.847	0.968

Explanation: The H_2-TPR of CuO is used to get the semi-quantitative assessment of different Cu species in Cu/SAPO-34. Especially, the Cu^+ contents are calculated as follows: amount of $Cu^+ = [H_2\ consumption_{(peak\,C)} + H_2\ consumption_{(peak\,D)} - H_2\ consumption_{(peak\,A)}]$.

those samples. The $Cu_{1.122}/Si_{0.106}Al_{0.532}$, owning the similar Cu loading with $Cu_{1.264}/Si_{0.374}Al_{0.441}$ sample, performs much lower SCR activity than that of $Cu_{1.264}/Si_{0.374}Al_{0.441}$, which is related to the less content of isolated Cu^{2+} species but the more bulk copper oxide in $Cu_{1.122}/Si_{0.106}Al_{0.532}$. And copper oxides are not active for SCR reaction [31,33,34].

Although the $Cu_{1.122}/Si_{0.106}Al_{0.532}$ sample has more isolated Cu^{2+} species than $Cu_{0.769}/Si_{0.130}Al_{0.435}$ in Fig. 12a, the $Cu_{1.122}/Si_{0.106}Al_{0.532}$ shows lower SCR activity. This may be due to the different environments or the location of the isolated Cu^{2+} ions which could also affect the SCR activities of catalysts. The EPR results in Fig. 6 show that the Cu species can migrate in Cu/SAPO-34 catalysts [25,26]. Uzunova et al. [51] reported that divalent cations preferred to locate on site (III) where they were stabilized by coordination to a higher number of framework oxygen atoms in SAPO-34.

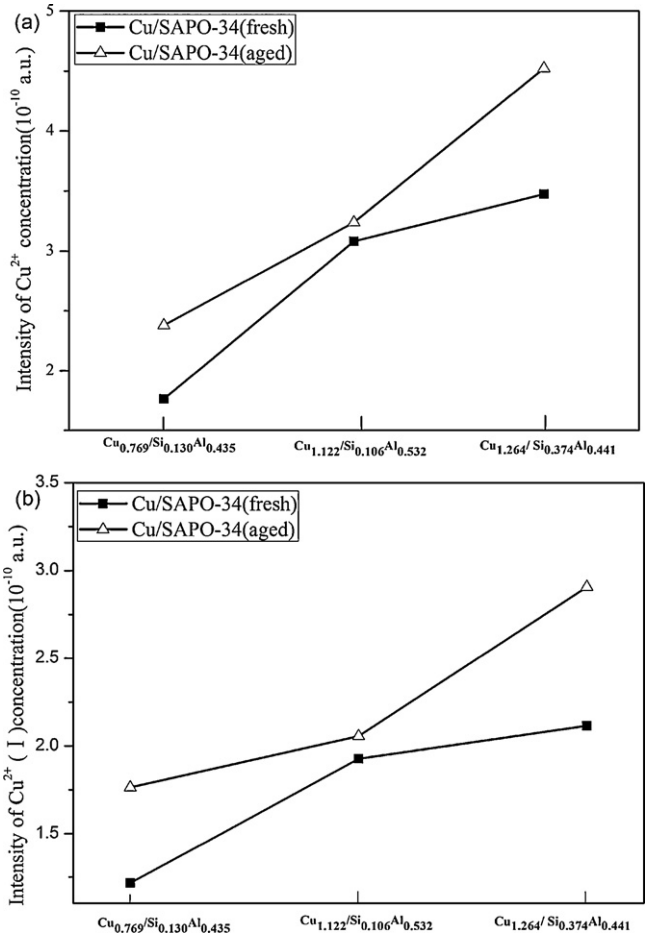

Fig. 12. The amount of isolated Cu^{2+} species (a) and isolated Cu^{2+} (I) species (b) calculated from the EPR spectra at normal temperature and pressure.

Table 7
The ratios of Cu^{2+} (I)/Cu^{2+} (III) from the EPR spectra after evacuation.

Sample	Cu^{2+} (I)/Cu^{2+} (III)	
	In fresh samples	In aged samples
$Cu_{0.769}/Si_{0.130}Al_{0.435}$	2.23	2.87
$Cu_{1.122}/Si_{0.106}Al_{0.532}$	1.67	1.74
$Cu_{1.264}/Si_{0.374}Al_{0.441}$	1.56	1.80

And the divalent cations can migrate to site (I) after adsorbing the NO. Lorena Picone [52] studied the SCR activity on Cu/SAPO SAT-7 and found that NO can adsorb on Cu^{2+} species at different sites. Kevan [25,26] found that two kinds of Cu^{2+} species were observed on dehydrated Cu/SAPO-34 catalysts after adsorbing gas molecule. It is deduced that the Cu^{2+} species may locate at site (I) and site (III) in the SCR reaction and it is known that Cu^{2+} species in site (III) may have less SCR activity than that in site (I) due to the steric hindrance [25,26]. Table 7 reflects the migration ability of isolated Cu^{2+} species in the evacuation during the EPR experiments. The $Cu_{1.122}/Si_{0.106}Al_{0.532}$ sample shows much more Cu^{2+} (III) species than that of $Cu_{0.769}/Si_{0.130}Al_{0.435}$, which results in its lower NO conversion. In addition, though the $Cu_{1.264}/Si_{0.374}Al_{0.441}$ has lower ratio of Cu^{2+} (I)/Cu^{2+} (III) than that of the $Cu_{0.769}/Si_{0.130}Al_{0.435}$ sample, the number of the isolated Cu^{2+} (I) species in $Cu_{1.264}/Si_{0.374}Al_{0.441}$ sample is higher as shown in Fig. 12b. So the $Cu_{1.264}/Si_{0.374}Al_{0.441}$ shows better NO conversion than $Cu_{0.769}/Si_{0.130}Al_{0.435}$. Fig. 12b shows that the content of the isolated Cu^{2+} in site (I) may not be the only reason for the different SCR activities of the Cu/SAPO-34 catalysts with various Si contents, as the $Cu_{1.122}/Si_{0.106}Al_{0.532}$ sample does not perform the better SCR activity than $Cu_{0.769}/Si_{0.130}Al_{0.435}$, even though there are more isolated Cu^{2+} (I) in the $Cu_{1.122}/Si_{0.106}Al_{0.532}$ sample.

The activities of aged Cu/SAPO-34 catalysts are summarized in Fig. 7. The SCR activities of all the aged Cu/SAPO-34 catalysts maintain or exceed the performance of the fresh samples, suggesting that the Cu/SAPO-34 catalysts have high thermal durability. The XRD, SEM and NMR spectra suggest that there is no obvious change of the structure in Cu/SAPO-34 after the hydrothermal treatment. The high stability of SAPO-34 molecular sieves kept the Cu species well dispersed. Moreover, the EPR and H_2-TPR results show that the amount of isolated Cu^{2+} species in the Cu/SAPO-34 catalysts increases after hydrothermal aging. The reducibility of Cu^{2+} species is also enhanced after hydrothermal aging, which is also contributed to the better NH_3-SCR activities on aged Cu/SAPO-34 catalysts.

5. Conclusions

The NH_3-SCR activities on Cu/SAPO-34 catalysts with various Si and Al contents have been investigated. The structure and the acidity of the support, Cu loading and the location of Cu^{2+} species,

all of which affected by the Si and Al contents, are closely related to the SCR performance over Cu/SAPO-34 catalysts.

The number of the acid sites in HSAPO-34 catalysts increases with the increasing Si contents when the mole ratio of the (Si + P)/Al is less than 1. The Si islands will be generated when the mole ratio of the (Si + P)/Al is bigger than 1. The formation of Si islands decreases the crystal size, the number of the acid sites and affects the strength of the acidity of HSAPO-34. In addition, the NO conversions on Cu/SAPO-34 are mainly related with the adsorption capacity ammonia of the catalysts at low temperature.

The Si and Al contents affect the contents of Cu^{2+} species. The contents of active sites are not the only reason deciding the activity over Cu/SAPO-34 samples with various Si contents, and the number of acid sites decided by Si content also affects their activities.

Due to the higher concentration of the isolated Cu^{2+} species and the better reducibility of the Cu^{2+} species in the aged catalysts, the aged Cu/SAPO-34 catalysts show the better SCR performance compared to the fresh samples.

Acknowledgements

The authors are grateful to the financial support from the GM Global Research & Development (RD-07-312-NV487). This work was supported by the program of the National High Technology Research and Development Program of China (863 Program, 2011AA03A405), the Program of Natural Science Foundation of China (No. 50972104), and the Key Program of Tianjin Natural Science Foundation (No. 09JCZDJC26600).

Appendix A. Supplementary data

Supplementary data associated with this article can be found, in the online version, at http://dx.doi.org/10.1016/j.apcatb.2012.08.016.

References

[1] G. Busca, L. Lietti, G. Ramis, F. Berti, Applied Catalysis B 18 (1998) 1–36.
[2] G. Centi, S. Perathoner, Applied Catalysis A 132 (1995) 179–259.
[3] M. Berggrund, H.H. Ingelsten, M. Skoglundh, A.E.C. Palmqvist, Catalysis Letters 130 (2009) 79–85.
[4] D.W. Fickel, E. D'Addio, J.A. Lauterbach, R.F. Lobo, Applied Catalysis B 102 (2011) 441–448.
[5] T. Ishihara, M. Kagawa, F. Hadama, Y. Takita, Journal of Catalysis 169 (1997) 93–102.
[6] Y. Watanabe, A. Koiwai, H. Takeuchi, S.A. Hyodo, S. Noda, Journal of Catalysis 143 (2) (1993) 430–436.
[7] S.T. Korhonen, D.W. Fickel, R.F. Lobo, B.M. Weckhuysen, A.M. Beale, Chemical Communications 47 (2011) 800–802.
[8] J.H. Kwak, R.G. Tonkyn, D.H. Kim, J. Szanyi, C.H.F. Peden, Journal of Catalysis 275 (2) (2010) 187–190.
[9] A. Buchholz, W. Wang, M. Xu, A. Arnold, M. Hunger, Microporous and Mesoporous Materials 56 (2002) 267–278.
[10] L. Xu, A. Du, Y. Wei, Y. Wang, Z. Yu, Y. He, X. Zhang, Z. Liu, Microporous and Mesoporous Materials 115 (2008) 332–337.
[11] J. Tan, Z. Liu, X. Bao, X. Liu, X. Han, Microporous and Mesoporous Materials 53 (2002) 97–108.
[12] E. Díaz, S. Ordóñez, A. Vega, J. Coca, Applied Catalysis B 56 (2005) 313–322.
[13] Z. Sarbak, M. Lewandowski, Applied Catalysis A 208 (2001) 317–321.
[14] T. Armaroli, L.J. Simon, M. Digne, T. Montanari, M. Bevilacqua, V. Valtchev, J. Patarin, G. Busca, Applied Catalysis A 306 (2006) 78–84.
[15] F. Benaliouche, Y. Boucheffa, P. Ayrault, S. Mignard, P. Magnoux, Microporous and Mesoporous Materials 111 (2008) 80–88.
[16] A. Izadbakhsh, F. Farhadi, F. Khorasheh, S. Sahebdelfar, M. Asadi, Y.Z. Feng, Applied Catalysis A 364 (2009) 48–56.
[17] Z. Yan, B. Chen, Y. Huang, Solid State Nuclear Magnetic Resonance 35 (2009) 49–60.
[18] G.A.V. Martins, G. Berlier, S. Coluccia, H.O. Pastore, G.B. Superti, G. Gatti, L. Marchese, Journal of Physical Chemistry C 111 (2007) 330–339.
[19] G. Sastre, D.W. Lewis, C.R.A. Catlow, Journal of Physical Chemistry B 101 (1997) 5249–5262.
[20] S. Ashtekar, S.V.V. Chilukuri, D.K. Chakrabarty, Journal of Physical Chemistry 98 (1994) 4878–4883.
[21] D. Zhang, Y. Wei, L. Xu, F. Chang, Z. Liu, S. Meng, B.L. Su, Z. Liu, Microporous and Mesoporous Materials 116 (2008) 684–692.
[22] G.A.V. Martins, G. Berlier, C. Bisio, S. Coluccia, H.O. Pastore, L. Marchese, Journal of Physical Chemistry C 112 (2008) 7193–7200.
[23] B. Onida, Z. Gabelica, J. Lourencüo, E. Garrone, Journal of Physical Chemistry 100 (1996) 11072–11079.
[24] S. Kieger, G. Delahay, B. Coq, B. Neveu, Journal of Catalysis 183 (1999) 267–280.
[25] M. Zamadies, X. Chen, L. Kevan, Journal of Physical Chemistry 96 (1992) 2652–2657.
[26] M. Zamadics, X. Chen, L. Kevan, Journal of Physical Chemistry 96 (1992) 5488–5491.
[27] A. Sultana, T. Nanba, M. Haneda, M. Sasaki, H. Hamada, Applied Catalysis B 101 (2010) 61–67.
[28] Y. Wan, J. Ma, Z. Wang, W. Zhou, S. Kaliaguine, Journal of Catalysis 227 (2004) 242–252.
[29] J.Y. Yan, G.D. Lei, W.M.H. Sachtler, H.H. Kung, Journal of Catalysis 161 (1996) 43–54.
[30] J.Y. Yan, W.M.H. Sachtler, H.H. Kung, Catalysis Today 33 (1997) 279–290.
[31] M. Richter, M.J.G. Fait, R. Eckelt, Applied Catalysis B 73 (2007) 269–281.
[32] C. Torre-Abreu, M.F. Ribeiro, C. Henriques, G. Delahay, Applied Catalysis B 12 (1997) 249–262.
[33] C. Torre-Abreu, M.F. Ribeiro, C. Henriques, G. Delahay, Applied Catalysis B 14 (1997) 261–272.
[34] R. Kefirov, A. Penkova, K. Hadjiivanov, S. Dzwigaj, M. Che, Microporous and Mesoporous Materials 116 (2008) 180–187.
[35] D. Berthomieu, G. Delahay, Chemical Reviews 48 (2006) 269–313.
[36] M. Richter, M.J.G. Fait, R. Eckelt, M. Schneider, J. Radnik, D. Heidemann, R. Fricke, Journal of Catalysis 245 (2007) 11–24.
[37] R. Bulánek, B. Wichterlová, Z. Sobalík, J. Tichy, Applied Catalysis B 31 (2001) 13–25.
[38] S. Kang, J.W. Bae, K. Woo, P.S.S. Prasad, K. Jun, Fuel Processing Technology 91 (2010) 399–403.
[39] P.J. Carl, D.E.W. Vaughan, D. Goldfarb, Journal of Physical Chemistry B 106 (2002) 5428–5437.
[40] P.J. Carl, S.C. Larsen, Journal of Physical Chemistry B 104 (2000) 6568–6575.
[41] M.W. Anderson, L. Kevan, Journal of Physical Chemistry 91 (1987) 4174–4179.
[42] C. Torre-Abreu, M.F. Ribeiro, C. Henriques, F.R. Ribeiro, Applied Catalysis B 11 (1997) 383–401.
[43] C. Torre-Abreu, M.F. Ribeiro, C. Henriques, F.R. Ribeiro, Applied Catalysis B 13 (1997) 251–264.
[44] J.Y. Luo, X. Hou, P. Wijayakoon, S.J. Schmieg, W. Li, W.S. Epling, Applied Catalysis B 102 (2011) 110–119.
[45] M. Devadas, O. Krocher, M. Elsener, A. Wokaun, G. Mitrikas, N. Soger, M. Pfeifer, Y. Demel, L. Mussmann, Catalysis Today 119 (2007) 137–144.
[46] S.C. Larsen, A. Aylor, A.T. Bell, J.A. Reimer, Journal of Physical Chemistry 98 (1994) 11533–11540.
[47] B.L. Trout, A.K. Chakraborty, A.T. Bell, Journal of Physical Chemistry 100 (1996) 17582–17592.
[48] T. Nanba, S. Masukawa, A. Ogata, J. Uchisawa, A. Obuchi, Applied Catalysis B 61 (2005) 288–296.
[49] M.H. Groothaert, K. Pierloot, A. Delabiey, R.A. Schoonheydt, Physical Chemistry Chemical Physics 5 (2003) 2135–2144.
[50] A.V. Kucherov, C.P. Hubbard, T.N. Kucherova, M. Shelef, Applied Catalysis B 7 (1996) 285–298.
[51] E.L. Uzunova, H. Mikosch, J. Hafner, Journal of Molecular Structure 912 (2009) 88–94.
[52] A. Lorena Picone, S.J. Warrender, A.M.Z. Slawin, D.M. Dawson, S.E. Ashbrook, P.A. Wright, S.P. Thompson, L. Gaberova, P.L. Llewellyn, B. Moulin, A. Vimont, M. Daturi, M.B. Park, S.K. Sung, I.S. Nam, S.B. Hong, Microporous and Mesoporous Materials 146 (2011) 36–47.